The Role of MRGPRX1 in the Melanogenesis of Human Primary Epidermal Melanocytes

Sae Woong Oh[1,5], Eunbi Yu[1,5], Kitae Kwon[1], Gyeonghyeon Kim[1], Hee Seon Shin[1], Seokhyeon Min[1], Yeonsoo Kim[1], Ki Wook Lee[4], Minkyung Song[2,5], Jae Youl Cho[3] and Jongsung Lee[1]

Journal of Investigative Dermatology (2025) ■, ■–■; doi:10.1016/j.jid.2025.09.016

MRGPRX1 (mas-related G protein-coupled receptor X1) is an orphan receptor, and its function in the skin cells remains unclear. In this study, we demonstrated *MRGPRX1* expression in skin cells, including melanocytes. We also found that *MRGPRX1* knockdown using short hairpin RNA increased melanin content, cellular tyrosinase activity, and the expression of melanogenic proteins, including tyrosinase, tyrosinase-related protein 2, and MITF in human epidermal melanocytes. In addition, *MRGPRX1* knockdown increased CRE-binding protein and p38 phosphorylation and decreased p44/42 phosphorylation. Furthermore, we demonstrated that chloroquine acts as an MRGPRX1 agonist. Specifically, in silico docking simulation showed that chloroquine binds to MRGPRX1. Chloroquine treatment increased MRGPRX1 expression, activation, and intracellular calcium influx. Unlike *MRGPRX1* knockdown, chloroquine treatment had antimelanogenic effects on melanin content, tyrosinase activity, melanogenic genes, and MAPKs. Furthermore, whereas chloroquine treatment increased calcium influx through TRPV1 and TRPA1, TRPA1 operated upstream of CRE-binding protein and p38 and activated them through calcium influx. We also found that *tert*-butyl hydroperoxide and UVA irradiation increased MRGPRX1 expression, suggesting that environmental factors affect MRGPRX1-mediated signaling. Collectively, these findings indicate that MRGPRX1-mediated signaling contributes to melanogenesis suppression, and chloroquine is a possible MRGPRX1 protein agonistic ligand, suggesting that MRGPRX1 could be a therapeutic target for pigmentary disorders.

Keywords: Chloroquine, CREB/p38 MAPK signaling, Melanogenesis, MRGPRX1, Pigmentation

INTRODUCTION

The MRGPR (mas-related GPCR) has 30–40% homology with MAS (Bader et al, 2014). MAS is an angiotensin-dependent receptor that modulates the angiotensin signaling pathway. MRGPR was first identified and shown to be primarily expressed in the dorsal root ganglia and is also known as a sensory neuron-specific receptor. It is currently named as the primate-specific MRGPRX according to the new nomenclature of MRGPRA, B, C, E, F, G, and H (Meixiong and Dong, 2017). On the basis of its structural homology with MAS, it was expected to be associated with the renin–angiotensin system, but the function of MRGPR was later found to be unrelated to the system (Poyner et al, 1990). Most MRGPR family members are associated with itching and pain. Human MRGPRX has been found in not only the dorsal root ganglia but also in other tissues, such as the testis and intestine. This contrasts the initial description of its expression only in the dorsal root ganglia; its expression in various tissues has been confirmed in recent studies (Bader et al, 2014; Kiatsurayanon et al, 2016; Tatemoto et al, 2006). Most MRGPR family members are orphan receptors, and their structures and functions have been studied. MRGPRX1 is a receptor that potentially binds to chloroquine, a well-known antimalarial drug that causes side effects such as vitiligo-like hypopigmentation. In addition, it causes skin itching and pain in response to chloroquine and the neuropeptide bovine adrenal medulla (BAM) 8-22 (Li et al, 2017). MRGPRX1 activation by chloroquine and BAM 8-22 causes human skin itching through MRGPRX-related signaling pathways. Studies on MRGPRX1 activation using these compounds suggested that skin itching may be mediated by a central/peripheral receptor. Hypopigmentation caused by chloroquine has been reported (Martín-García et al, 2003), and the chloroquine-induced pigment disorder is known as vitiligo-like hypopigmentation. Chloroquine was previously reported to not affect tyrosinase protein in vitro (Dupré et al,

[1]*Molecular Dermatology Laboratory, Department of Integrative Biotechnology, College of Biotechnology and Bioengineering, Sungkyunkwan University, Suwon City, Korea;* [2]*Integrative Research of T cells Laboratory, Department of Integrative Biotechnology, College of Biotechnology and Bioengineering, Department of Biopharmaceutical Convergence, Sungkyunkwan University, Suwon City, Korea;* [3]*Molecular Immunology Laboratory, Department of Integrative Biotechnology, College of Biotechnology and Bioengineering, Sungkyunkwan University, Suwon City, Korea; and* [4]*RNA-based Precision Medicine Laboratory, Department of Integrative Biotechnology, College of Biotechnology and Bioengineering, Sungkyunkwan University, Suwon City, Korea*

[5]*These authors contributed equally to this work.*

Correspondence: Jongsung Lee, Department of Integrative Biotechnology, College of Biotechnology and Bioengineering, Sungkyunkwan University, 2066 Seobu-Ro, Jangan-Gu, Suwon 16419, Korea. E-mail: bioneer@skku.edu and Jae Youl Cho, Department of Integrative Biotechnology, College of Biotechnology and Bioengineering, Sungkyunkwan University, 2066 Seobu-Ro, Jangan-Gu, Suwon 16419, Korea. E-mail: jaecho@skku.edu

Abbreviations: BAM, bovine adrenal medulla; CREB, CRE-binding protein; FK, forskolin; HEK293T, human embryonic kidney 293T; HEM, human epidermal melanocyte; MC1R, melanocortin 1 receptor; shMRGPRX1, MRGPRX1-targeted short hairpin RNA; TBHP, tert-butyl hydroperoxide

Received 23 April 2025; revised 5 September 2025; accepted 5 September 2025; accepted manuscript published online XXX; corrected published online XXX

1985; Saunders et al, 1959); however, it could affect the change in enzyme activity in the presence of copper (Bowness and Morton, 1953; Selvaag, 1997). In addition, a photopatch test suggested that melanocyte toxicity could be increased through chloroquine-induced photosensitivity (Selvaag, 1997). However, the mechanism of chloroquine-induced hypopigmentation has not been clearly elucidated, even though hypopigmentation is a known side effect of chloroquine. Therefore, in this study, we investigated the function of MRGPRX1 in melanogenesis and elucidated its signaling mechanisms in human epidermal melanocytes (HEMs). In addition, we demonstrated the possibility of chloroquine being an agonistic ligand of MRGPRX1 and investigated whether chloroquine-induced hypopigmentation occurs through MRGPRX.

RESULTS

MRGPRX1 expression in human skin cells

MRGPRX family proteins have previously been identified as neuron-specific receptors; however, they are expressed in various organs, such as the urinary bladder, lungs, adipose tissue, and testes (Al Hamwi et al, 2022). Because its expression in human epidermal cells has not been reported, we investigated *MRGPRX1* expression in HEMs and human primary epidermal keratinocytes. RT-PCR revealed that *MRGPRX1* was expressed in both HEMs and human primary epidermal keratinocytes (Figure 1a).

MRGPRX1 regulates melanogenesis in HEM

To examine the function of MRGPRX1 in melanocytes, we investigated melanogenesis under *MRGPRX1*-knockdown conditions using short hairpin RNA viral particle transduction. The *MRGPRX1* mRNA levels were significantly reduced in the knockdown control using *MRGPRX1*-targeted short hairpin RNA (shMRGPRX1) (Figure 1b). Both melanin content (Figure 1c) and tyrosinase activity (Figure 1d) were also significantly increased in the *MRGPRX1*-knockdown group compared with those in the mock group. In addition, immunoblotting analysis demonstrated that although MRGPRX1 protein levels were knocked down in the sh*MRGPRX1* group, those of melanogenic genes, such as MITF, tyrosinase, and tyrosinase-related protein (TRP)2, were increased. However, the TRP1 protein levels were unaffected (Figure 1e). The p38 and p44/42 MAPK phosphorylation levels increased and decreased, respectively. The phosphorylation levels of CRE-binding protein (CREB), which regulates MITF expression, also increased (Figure 1e). Densitometric analyses for Figure 1e are shown in Figure 1f. These data indicate that *MRGPRX1* knockdown contributes to melanogenesis, suggesting that MRGPRX1 is involved in suppressing the melanogenic signaling. Furthermore, the FLUO-4 assay, which determines calcium flux, showed a decrease in calcium flux in the sh*MRGPRX1* group compared with that in the mock group, indicating that the function of MRGPRX1 is related to the intracellular calcium response (Figure 1g).

Chloroquine acts as a possible ligand for MRGPRX1

Chloroquine causes human skin itching through MRGPRX-related signaling pathways (Meixiong and Dong, 2017). Therefore, we examined the interaction between MRGPRX1 and chloroquine using the AutoDock virtual ligand screening software (Morris et al, 2009; Trott and Olson, 2010). First, screening using the AutoDock method was conducted using the melanocortin 1 receptor (MC1R) and forskolin (FK), which are known melanogenesis-activating receptors and ligand molecules, respectively (D'Orazio et al, 2006). The 3-dimensional structure of MC1R obtained from the Protein Data Bank database was used. The structure in PubChem (Compound Identification: 47936) was used as the 3-dimensional structure of FK. On the basis of the result obtained with AutoDock, binding affinity of MC1R and FK was -6.4 ± 0.32 kcal/mol. Although α-melanocyte-stimulating hormone is a ligand of MC1R, FK induces melanogenesis more strongly than α-melanocyte-stimulating hormone. After verifying the receptor–ligand affinity using MC1R and FK, the binding affinities of chloroquine and MRGPRX1 were measured. The protein 3-dimensional structure of MRGPRX1 was obtained from an alpha-fold protein database. The 3-dimensional structure of chloroquine was obtained from PubChem (Compound Identification: 2719). The binding affinity of MRGPRX1 and chloroquine using AutoDockTools was -4.19 ± 0.27 kcal/mol, 3.62 ± 1.63 rmsd/ub, and 2.13 ± 0.85 rmsd/lb (Figure 2a). Although their binding affinities were lower than those of MC1R and FK, the binding affinities of MRGPRX1 and chloroquine were considerably higher, suggesting that MRGPRX1 interacted with chloroquine.

Chloroquine induces MRGPRX1 activation

To investigate whether chloroquine acts as an agonist of MRGPRX1, we used the PRESTO-TANGO assay system, which enables the detection of G-protein coupled receptor activation through β-arrestin recruitment and luciferase reporter expression. Using this system, we assessed the ability of chloroquine to activate MRGPRX1 in human embryonic kidney 293T (HEK293T) cells. We investigated whether chloroquine induces calcium influx in HEK293T cells. Immunofluorescence assays showed increased FLAG expression, indicating proper transfection (Figure 2b). We also found that chloroquine increased the calcium influx in both transfected HEK293T cells and melanocytes (Figure 2c and d). To verify MRGPRX1 activation, we measured its receptor activity using a luciferase assay. BAM8-22, an MRGPRX1 activator, was also used as a positive control and compared with chloroquine. The results showed that chloroquine significantly increased MRGPRX1 activation in a concentration-dependent manner (Figure 2e). The 10-μM chloroquine-induced MRGPRX1 activation was more than 5 times higher than that using 10 μM of BAM8-22. These results indicated that chloroquine could activate MRGPRX1 by acting as an agonist. To investigate functionally critical residues of MRGPRX1, we performed structure-guided mutagenesis informed by in silico energy modeling. Molecular docking highlighted glutamate 157 and tyrosine 99 as key residues, which were mutated to arginine (E157R) and alanine (Y99A), respectively, to disrupt charge or aromatic interactions (Figure 2f). The data in Figure 2f were based on in silico analysis, not experimental data. Using the PRESTO-TANGO system with a TET-inducible luciferase reporter, we also found that both mutants markedly reduced luciferase activity compared with wild type, indicating impaired G-

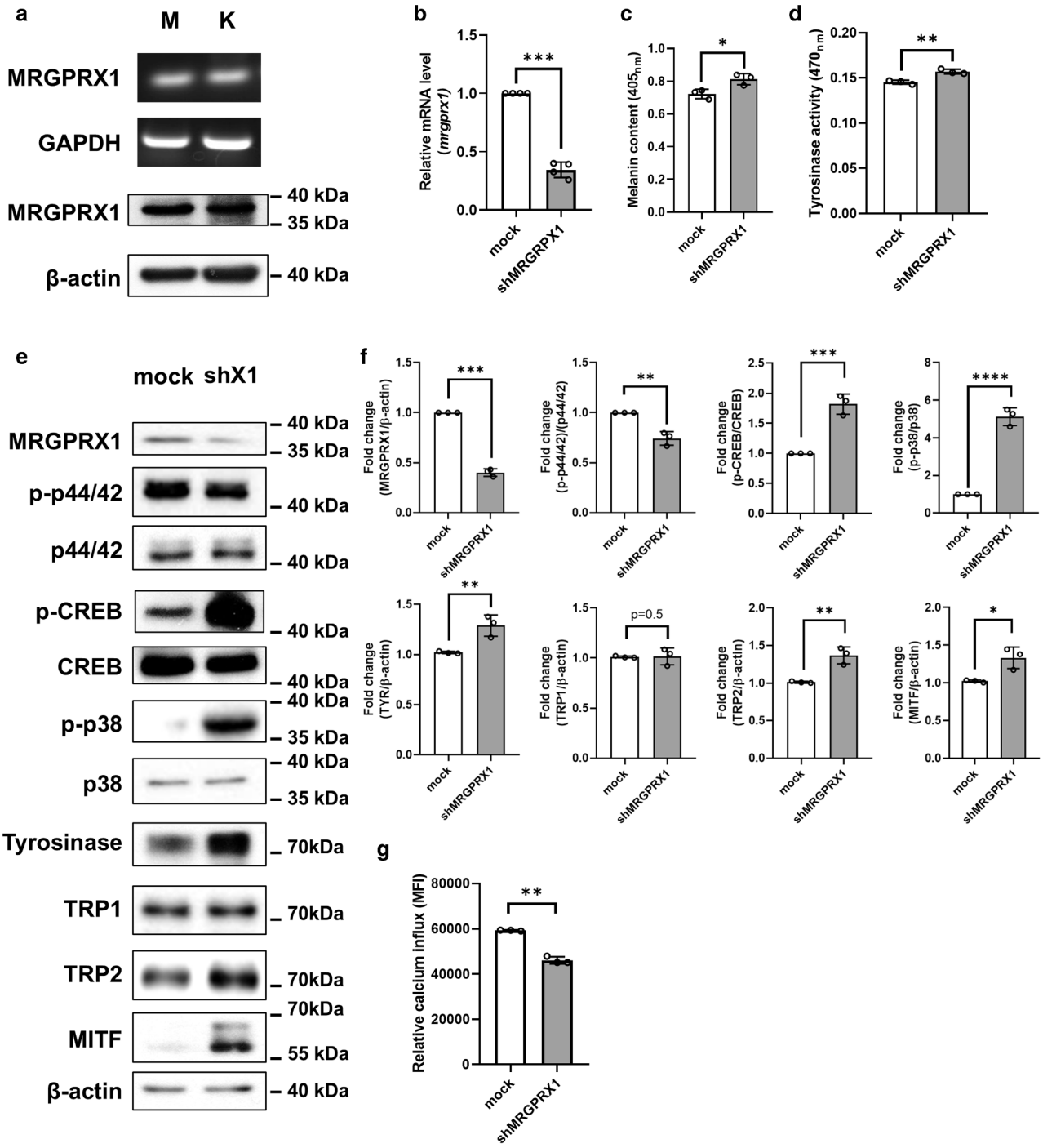

Figure 1. Human MRGPRX1 is expressed in human skin cells and regulates melanogenesis in HEMs. **(a)** RT-PCR SYBR agarose gel analysis (upper panel) of *MRGPRX1* mRNA and immunoblotting analysis (lower panel) of MRGPRX1 protein. *MRGPRX1* mRNA expression and MRGPRX1 protein expression were identified in HEMs and human epidermal keratinocytes. M denotes melanocytes, and K denotes keratinocytes. **(b)** After sh*MRGPRX1* transduction, knockdown of *MRGPRX1* was confirmed using RT-qPCR. *MRGPRX1* mRNA levels were reduced in the shMRGPRX1-transduced group. ***$P < .001$ versus mock group. **(c, d)** Melanin content and tyrosinase activity in sh*MRGPRX1* and mock groups. *$P < .05$ and **$P < .01$ versus mock group. **(e)** Results of immunoblotting of melanogenic proteins and p38, p44/42, and CREB phosphorylation. shX1 denotes sh*MRGPRX1*. **(f)** Densitometric analysis of immunoblotting. **(g)** Results of the FLUO-4 experiment. **$P < .01$ versus mock group. Immunoblotting quantifications were based on at least 3 independent experiments. CREB, CRE-binding protein; HEM, human epidermal melanocyte; ns, not significant; sh*MRGPRX1*, *MRGPRX1*-targeted short hairpin RNA.

protein coupled receptor signaling. These results validate computational predictions and underscore the essential role of these residues in MRGPRX1-dependent transcriptional activity, potentially linked to melanogenesis (Figure 2g).

Chloroquine inhibits melanogenesis by regulating CREB and MAPKs in HEMs

Although chloroquine induces side effects, such as vitiligo-like skin hypopigmentation (Martín-García et al, 2003), the

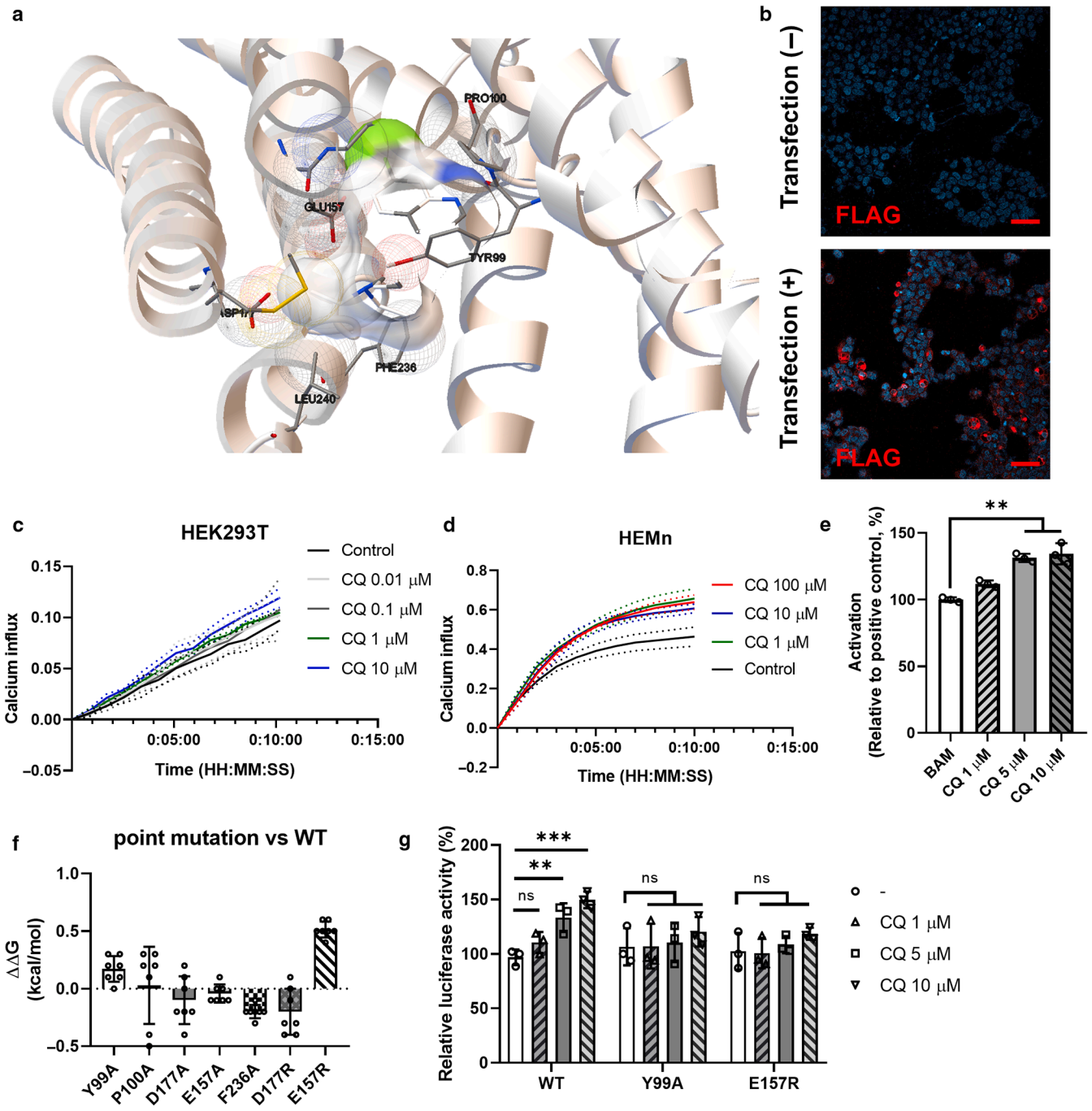

Figure 2. In silico analysis using virtual ligand screening. Chloroquine induces calcium influx and MRGPRX1 activation in HEK293T cells. **(a)** Image schematic of the results of the AutoDock tools analysis. The image shows the highest possible interaction residue. **(b)** Transfection with MRGPRX1-Tango plasmid DNA with FLAG tag was confirmed using immunofluorescence. Red fluorescence indicates FLAG. Bar = 50 μm. **(c)** HEK293T cells were treated with chloroquine at the indicated concentrations and confirmed using FLUO-4 assay. Data are presented as mean values, with dotted lines indicating ±SD. **(d)** HEMs were treated with chloroquine at the indicated concentrations and confirmed using FLUO-4 assay. Data are presented as mean values, with dotted lines indicating ±SD. **(e)** MRGPRX1 receptor activity was confirmed using the PRESTO-TANGO system. $^{**}P < .01$ versus 10 μM BAM 8-22 (BAM) treatment group. (**f**) Predicted binding affinity changes of MRGPRX1 single-nucleotide variants relative to WT protein. In silico analysis was performed to evaluate the effect of individual single-nucleotide variants in MRGPRX1 on the binding affinity (ΔΔG, kcal/mol) for chloroquine. Positive ΔΔG values indicate reduced binding stability relative to the WT receptor, whereas negative values suggest increased stability. $^{**}P < .01$ versus wT group. **(g)** MRGPRX1 receptor activity was confirmed using the PRESTO-TANGO system with WT MRGPRX1 and 2-point mutants (Y99A, E157R) to assess chloroquine-induced receptor activity. Cells were treated with increasing concentrations of chloroquine (1, 5, and 10 μM), and luciferase activity was normalized to β-galactosidase expression. WT MRGPRX1 exhibited a dose-dependent increase in activity upon chloroquine treatment, whereas both Y99A and E157R mutants showed no significant chloroquine-induced activation. $^{**}P < .01$ and $^{***}P < .001$ versus control group. β-gal, β-galactosidase; BAM, bovine adrenal medulla; HEK293T, human embryonic kidney 293T; HEM, human epidermal melanocyte; ns, not significant; WT, wild-type.

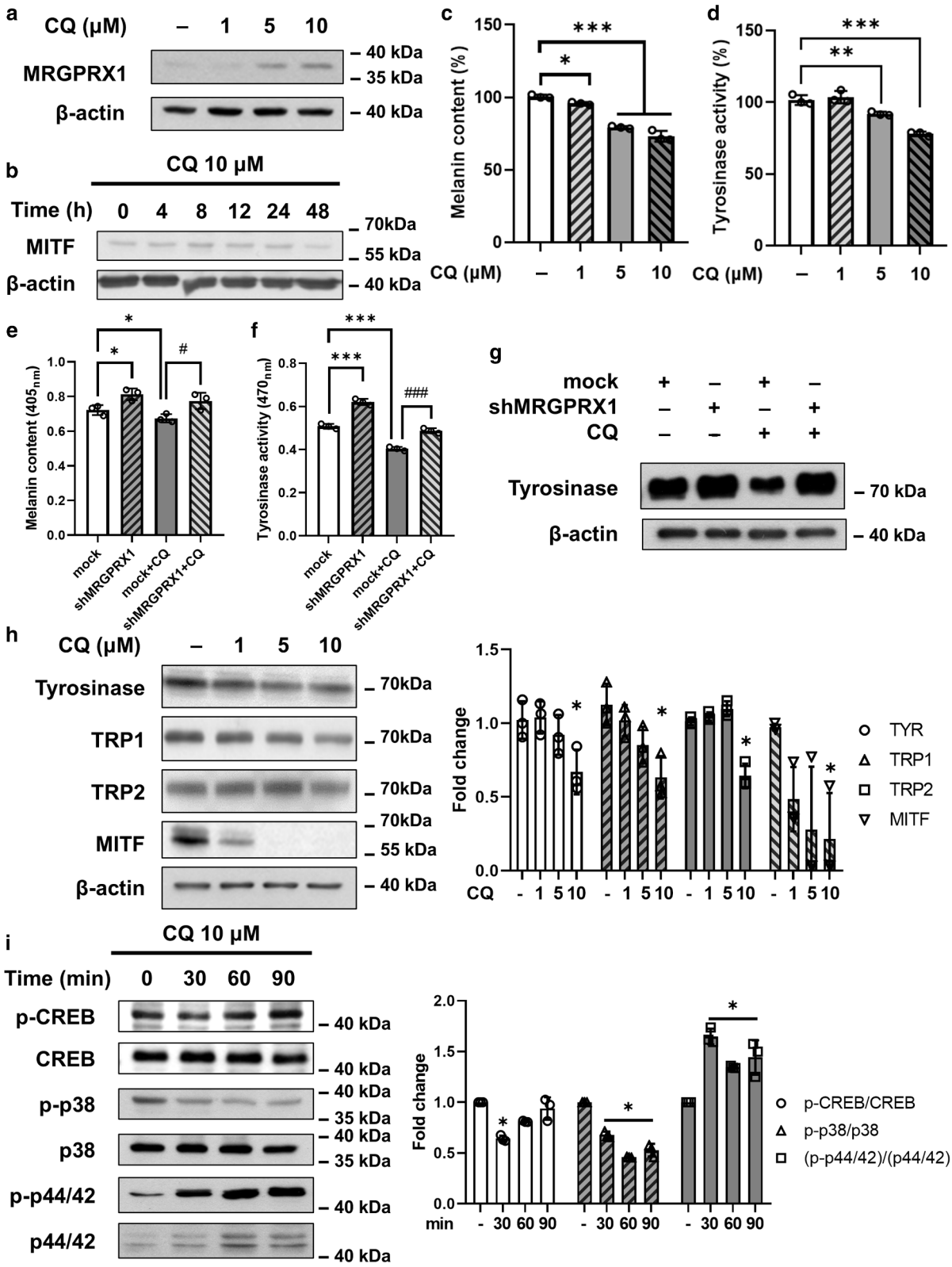

Figure 3. CQ increases MRGPRX1 expression and regulates melanogenic protein expression and phosphorylation in epidermal melanocytes. **(a)** MRGPRX1 immunoblotting results. MRGPRX1 expression increased with CQ concentration. **(b)** MITF expression decreased over time upon hourly treatment with 10 μM CQ. **(c, d)** Melanin content and tyrosinase activity after 48-h treatment with the indicated CQ concentrations. CQ decreased melanin content and tyrosinase activity in a concentration-dependent manner. **(e)** Melanin content after sh*MRGPRX1* transduction. HEMs were transfected with short hairpin RNA and treated with 10 μM CQ for 48 h. *$P < .05$ versus mock group. #$P < .05$ versus mock + CQ group. **(f)** Tyrosinase activity after sh*MRGPRX1* transduction. HEMs were transfected with short hairpin RNA and treated with 10 μM CQ for 48 h. ***$P < .001$ versus mock group. ###$P < .001$ versus mock + CQ group. **(g)** Tyrosinase immunoblotting results after sh*MRGPRX1* transduction. HEMs were transfected with short hairpin RNA and treated with 10 μM CQ for 48 h. **(h)** Results of melanogenic protein immunoblotting. The indicated CQ concentrations were determined after 48 h of treatment. The expression of tyrosinase, TRP1,

mechanisms of chloroquine-induced hypopigmentation have not been clearly elucidated. Therefore, we examined the effect of chloroquine on MRGPRX1 expression. Chloroquine treatment increased the protein level of MRGPRX1 in a concentration-dependent manner and decreased the protein level of MITF, a master regulator of melanogenesis. (Figure 3a and b). Furthermore, chloroquine treatment decreased melanin content (Figure 3c) and cellular tyrosinase activity in a concentration-dependent manner (Figure 3c and d). However, *MRGPRX1* knockdown attenuated the effects of chloroquine on melanin content, tyrosinase activity, and protein expression (Figure 3e–g and Supplementary Figure S1). These results indicated that chloroquine exerts its antimelanogenic activity in a MRGPRX1-dependent manner. Moreover, chloroquine treatment reduced tyrosinase, TRP1, TRP2, and MITF protein levels in a concentration-dependent manner (Figure 3h). The phosphorylation levels of melanogenesis signaling pathway–related proteins were also investigated. Unlike *MRGPRX1* knockdown, chloroquine treatment increased p44/42 phosphorylation (Figure 3h). This is consistent with the results of a previous report showing that MRGPRX1 is associated with p44/42 activation in neuron-derived cells (Solinski et al, 2013). In addition, the phosphorylation levels of CREB and p38, which induce MITF expression (Hwang et al, 2019), decreased after chloroquine treatment at 30-minute condition (Figure 3i). These data indicate that chloroquine inhibits melanogenesis, and its mechanism of action is associated with MRGPRX1.

Chloroquine inhibits CREB/MAPK signaling and autophagic flux through calcium-mediated signaling through TRPA1

We have previously demonstrated that chloroquine treatment reduced CREB phosphorylation in HEMs. To verify this, we performed a CRE luciferase reporter assay using HEK293T cells transiently transfected with MRGPRX1 plasmid. Chloroquine treatment reduced CRE luciferase reporter activity. In addition, MDL12330A (an adenylate cyclase inhibitor), a positive control, reduced the CRE luciferase reporter activity (Figure 4a). These results confirmed that chloroquine inhibits melanogenesis by regulating CRE signaling through interaction with MRGPRX1. A previous study has reported that neurotransmission by MRGPRX occurs through TRPV1 and TRPA1 activation (Imamachi et al, 2009). TRPV1 and TRPA1 are important channels that regulate calcium ion concentration gradients during neuronal activity; however, their roles in melanocytes are not clearly understood. In a calcium flux experiment using specific TRPV1 and TRPA1 inhibitors, we found that the chloroquine-induced calcium flux was reduced by the TRPV1 inhibitor BCTC and the TRPA1 inhibitor A967079. In particular, the effect of BCTC on chloroquine-induced calcium influx was greater than that of A967079 (Figure 4b). These results suggest that TRPV1 and TRPA1 contribute to the effects of chloroquine on melanogenesis. However, the reduced p38 and CREB phosphorylation levels after chloroquine treatment were recovered for A967079 but not for BCTC (Figure 4c and d). In addition, although p44/42 phosphorylation levels increased in the chloroquine-treated group, A967079 attenuated the effects of chloroquine (Figure 4c and d). However, BCTC did not alter the effect of chloroquine on p44/42. Collectively, these data indicated that chloroquine inhibited melanogenesis by regulating CREB and MAPK signaling through TRPA1-dependent calcium signaling. Proteomic stress caused by autophagy defects leads to cellular dysfunction (Srivastav et al, 2024). Therefore, we evaluated chloroquine-induced autophagy changes in MRGPRX1-expressed HEK293T cells and the involvement of BCTC and A967079 in these changes. Although the GFP signal decreased in the chloroquine-treated group than the RFP signal, which was an internal control, the decreased GFP signal in the chloroquine-treated group was increased using A967079 but not BCTC (Figure 4e and f). The results are shown in a graph by measuring the mean fluorescence intensity (Figure 4f). These results indicated that chloroquine increased autophagic flux through TRPA1-dependent calcium signaling.

UVA and *tert*-butyl hydroperoxide affect MRGPRX1 expression

We examined whether environmental stress affected MRGPRX1 expression and activity. Therefore, stimulation with UVA and *tert*-butyl hydroperoxide (TBHP) were used to determine the changes in MRGPRX1 and MITF protein expressions. Although 12 J UVA irradiation reduced MRGPRX1 expression, MITF protein levels increased (Figure 5a and b). However, TBHP increased MRGPRX1 and reduced MITF protein levels. These results indicate that UVA and TBHP have opposing effects on MRGPRX1 and MITF expression.

Gene expression changes by *MRGPRX1* knockdown implicate upstream regulators of MITF and Wnt signaling in MRGPRX1-dependent pigmentary networks

To investigate the transcriptomic changes induced by *shMRGPRX1*, we first performed differential gene expression analysis using RNA-sequencing data. Volcano plot analysis revealed a substantial number of genes exhibiting statistically significant expression changes. Genes with $\log_2$ fold change >1 and $P < .05$ were considered significantly upregulated (red), whereas genes with a $\log_2$ fold change < -1 and $P < .05$ were considered significantly downregulated (blue), and genes with a nonsignificant fold change ($-1 < \log_2$ fold change < 1) but a $P < .05$ were considered weakly regulated (black) (Figure 6a). $P < .05$ was considered significant. The set of genes was visualized in a diagram (Figure 6b). Transcript abundance for each gene was quantified as transcripts per kilobase million, enabling normalization across different genes and samples. To better understand the biological relevance of these differentially expressed genes, we performed Gene Ontology enrichment analysis (Figure 6c and d). The most enriched terms included "DNA binding," "intracellular signal transduction," and "vesicle-mediated

TRP2, and MITF was decreased in a CQ concentration-dependent manner. The graphs on the right show the results of band intensity densitometry. *$P < .05$ versus control group. **(i)** Immunoblotting results of p38, p44/42, and CREB phosphorylation after treatment with 10 μM CQ for the indicated periods. p44/42 phosphorylation increased, and p38 and CREB phosphorylation decreased. The graph on the right indicates band intensity densitometry and normalized by total protein for each sample. Immunoblotting quantifications were based on at least 3 independent experiments. *$P < .05$ versus control group. CQ, chloroquine; CREB, CRE-binding protein; h, hour; HEM, human epidermal melanocyte; sh*MRGPRX1*, *MRGPRX1*-targeted short hairpin RNA; TRP, tyrosinase-related protein.

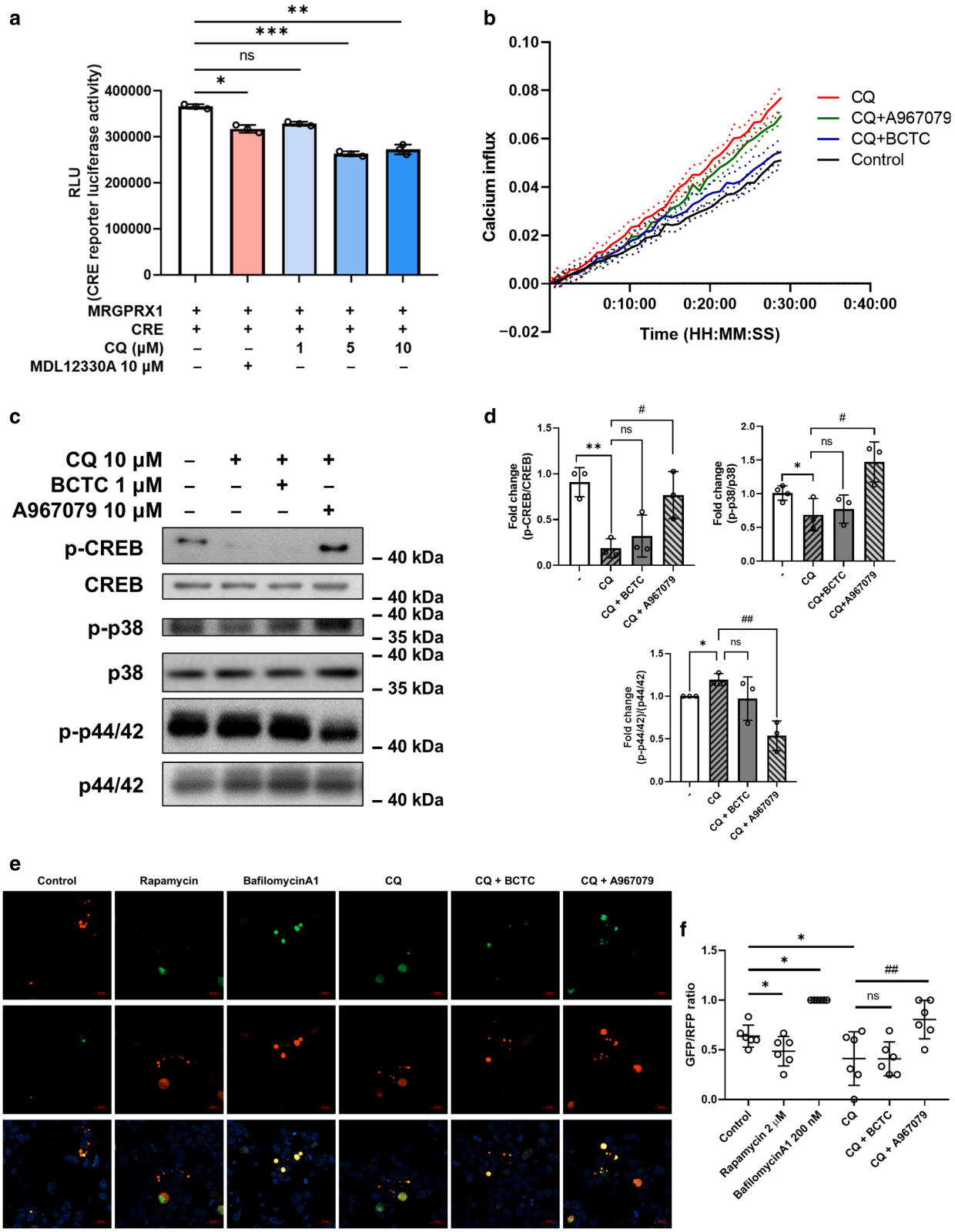

Figure 4. Chloroquine inhibits melanogenesis through calcium channel–mediated signaling pathways. (**a**) CRE reporter activity was confirmed in HEK293T cells. *MRGPRX1*, CRE luciferase, and β-gal plasmid DNA were transfected together. CRE reporter activity decreased in the MDL12330A, 5 μM chloroquine, and 10 μM chloroquine treatment groups. $^{*}P < .05$ versus control group. $^{**}P < .01$ versus control group. $^{***}P < .001$ versus control group. **(b)** Confirmation of FLUO-4 assay under chloroquine cotreatment with TRPV1 and TRPA1 inhibitor. BCTC (TRPV1-specific antagonist) and A967079 (TRPA1 inhibitor) treatment attenuated the chloroquine-induced increase in calcium influx. **(c)** Immunoblotting results of p38, p44/42, and CREB phosphorylation. HEMs were treated with 10 μM chloroquine for 90 minutes and cotreated with 1 μM BCTC or 10 μM A967079. **(d)** Densitometric analysis for **c**. **(e)** Autophagic flux detection by immunofluorescence. Red and green fluorescence indicate internal control RFP-LC3ΔG and autophagic flux GFP-LC3, respectively. Bar = 20 μm. **(f)** Calculated

transport"—highlighted functional annotations associated with melanocyte biology, including transcriptional regulation, and melanosome biogenesis. In addition, we also performed a focused selection of melanogenesis-related genes on the basis of prior biological knowledge. This approach, which integrates statistical filtering and pathway relevance, provides a more comprehensive interpretation of how pigmentation pathways respond to environmental stress. It is also able to facilitate the identification of candidate genes for further functional validation. These genes were identified through prior literature and pathway annotations and then ordered in descending $\log_2$ fold change to highlight those exhibiting the greatest transcriptional differences under the experimental conditions (Supplementary Table S1). The resulting list includes key regulators of melanocyte physiology, melanosome biogenesis and transport (DCT and TYRP1), and pigmentation-associated protein expressions (CTNNB1 and MITF). Notably, *MITF*, a central transcription factor in melanocyte, appeared among the most upregulated genes. Despite some entries not meeting conventional cutoffs for significance, the inclusion of these genes enables a biologically informed interpretation of pigmentation-related transcriptional dynamics. This approach complements global differential expression analysis by capturing pathway-specific responses potentially masked in purely statistical filtering.

Complementary STRING-based enrichment highlighted significant associations with skin-specific expression profiles and phosphoprotein-related molecular functions, suggesting functional relevance at the gene level despite the lack of pathway-level Gene Ontology enrichment (Supplementary Figure S2). A detailed investigation of melanogenesis-related genes has revealed a substantial upregulation of *MITF* and its downstream targets in response to MRGPRX1 knockdown (Supplementary Table S1). This observation provides further evidence for the hypothesis that MRGPRX1 suppresses melanogenesis through the downregulation of MITF-mediated signaling. Furthermore, this targeted analysis highlights the value of RNA sequencing in identifying biologically relevant transcriptional changes within melanogenesis pathways.

DISCUSSION

MRGPRX1 function and expression in human melanocytes remain unknown. Although chloroquine causes vitiligo as a side effect, its mechanism of action remains unclear (Martín-García et al, 2003). In this study, we demonstrated the involvement of MRGPRX1-mediated signaling pathway in chloroquine-induced vitiligo-like hypopigmentation. In addition, we demonstrated sufficient binding of chloroquine to MRGPRX1 using in silico docking and chloroquine-induced MRGPRX1 activation using the PRESTO-TANGO luciferase assay, indicating that chloroquine acts as an MRGPRX1 agonist. These results are also supported by the results of a previous study, reporting that chloroquine acts as a potential ligand for MRGPRX1 (Bader et al, 2014). We also demonstrated MRGPRX1 expression in skin cells and its effects on cell physiology. We found that reducing MRGPRX1 expression increased melanogenesis in a knockdown study using shMRGPRX1. In addition, we confirmed that MRGPRX1 expression is involved in melanogenesis regulation. Specifically, during MRGPRX1 activation by chloroquine, we found that MRGPRX1 expression changed depending on chloroquine concentration. Although MRGPRX1 regulates calcium ion concentration through cell membrane calcium channels, its function as a G-protein coupled receptor has not been clearly identified yet (Meixiong and Dong, 2017). In this study, we found that chloroquine-activated MRGPRX1 induced calcium influx through TRPV1 or TRPA1 channels, which was inhibited by TRPV1- and TRPA1-specific inhibitors. To investigate how TRPV1 and TRPA1 activation affects melanogenesis, we performed immunoblotting after cotreatment with chloroquine and inhibitors (TRPV1 and TRPA1) and found that chloroquine treatment reduced p38 and CREB phosphorylation levels. In addition, although the TRPA1 inhibitor A967079 attenuated the effect of chloroquine on CREB and p38 phosphorylation, the TRPV1 inhibitor BCTC did not affect the effect of chloroquine on CREB and p38 phosphorylation, suggesting that TRPA1 contributes to chloroquine-induced hypopigmentation. These results indicate that TRPA1 participates in the chloroquine-induced inhibition of melanogenesis and suggest that chloroquine-induced antimelanogenesis is mediated by the MRGPRX1—TRPA1—CREB/p38 signaling pathway. Chloroquine is a well-known antimalarial drug that causes side effects, such as skin itching. Chloroquine also causes vitiligo-like hypopigmentation (Martín-García et al, 2003). Our finding that chloroquine acts as a ligand for MRGPRX1 and inhibits melanogenesis in melanocytes provides a further understanding for treating cutaneous vitiligo. In addition, *MRGPRX1* expression in various tissues, including nerves, has recently been reported; however, research on its function is insufficient. Our findings contribute to a clear understanding of the roles of MRGPRX1 in different cell types. Integrated analysis of the mock and shMRGPRX1 treatment groups suggested that reduced MRGPRX1 expression leads to transcriptional changes indicative of increased melanogenesis. Specifically, MRGPRX1 acts as a negative regulator that interferes with key signaling pathways involved in melanin synthesis in melanocytes, including the Wnt/β-catenin, cAMP/CREB, and MAPK pathways. MRGPRX1 knockdown likely relieves its suppressive influence on these pathways, resulting in increased MITF expression and activity; increased expression of tyrosinase-related enzymes; and ultimately, increased melanin production. Biologically, this indicates that under normal conditions, MRGPRX1 inhibits melanogenic signaling, thereby limiting melanin synthesis. In particular, the Wnt signaling activation and MITF—tyrosinase axis upregulation observed after MRGPRX1 suppression strongly support the hypothesis that MRGPRX1 serves as an upstream inhibitor of melanin production. Although MRGPRX1 has primarily been studied as a pruriceptive (itch-related) receptor, this study revealed, to our knowledge, previously unreported role for MRGPRX1 in

GFP and RFP ratio using mean fluorescence intensity of the images. Immunoblotting quantifications were based on at least 3 independent experiments. CREB, CRE-binding protein; HEK293T, human embryonic kidney 293T; HEM, human epidermal melanocyte.

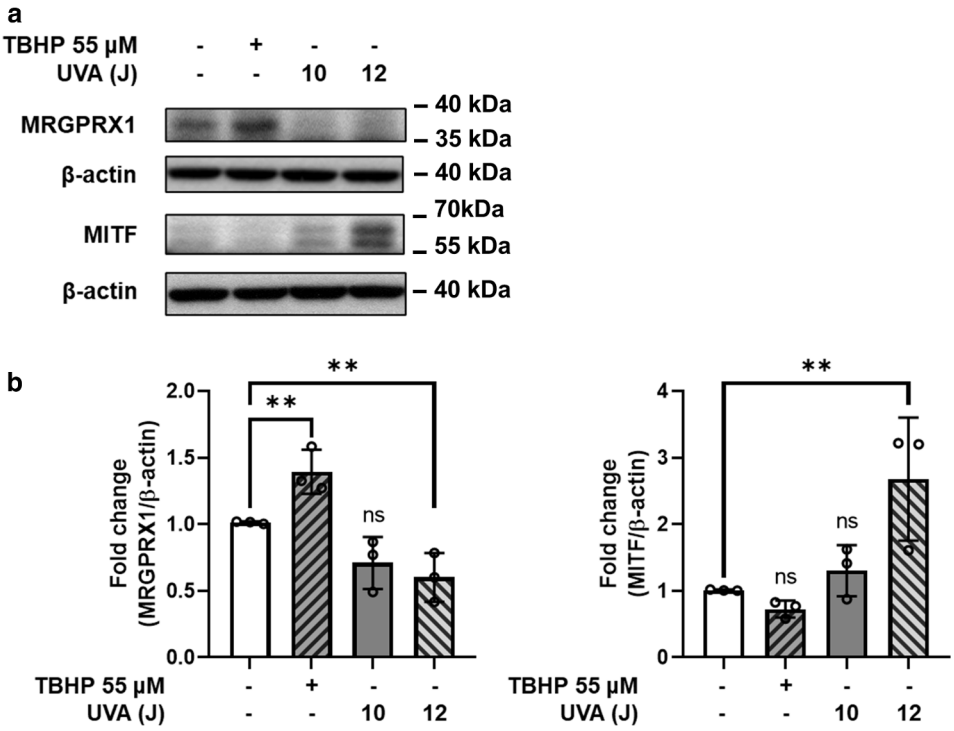

Figure 5. UVA and TBHP regulate MRGPRX1 expression. (a) Immunoblotting results of MRGPRX1 and MITF. HEMs were treated with TBHP or irradiated by UVA. **(b)** The graphs indicate the band intensity densitometry. $*P < .05$ versus control group. $**P < .01$ versus control group. Immunoblotting quantifications were based on at least 3 independent experiments. HEM, human epidermal melanocyte; TBHP, tert-butyl hydroperoxide.

pigmentation biology. For example, if MRGPRX1 signaling attenuates responses to melanogenic stimuli, such as γ-melanocyte-stimulating hormone, its suppression may prevent inhibitory control and promote melanocyte activity. This suggests the existence of a neurocutaneous feedback mechanism, where MRGPRX1 signaling integrates environmental or neural cues to modulate skin pigmentation. The observed increase in melanogenesis upon MRGPRX1 knockdown highlights its potential as a therapeutic target for conditions characterized by pigment deficiency, such as vitiligo or postinflammatory hypopigmentation. Conversely, MRGPRX1 activation could serve as a strategy to treat hyperpigmentation disorders, such as melasma or solar lentigines, by suppressing excessive melanin production. Modulating MRGPRX1 activity may achieve the controlled regulation of melanogenesis, providing therapeutic benefits for both hypo and hyperpigmentation-related skin conditions. Finally, excess MRGPRX1 activity may contribute to hypopigmented conditions and thus represent a biomarker or intervention point in depigmentation disorders. In conclusion, the differences in gene expression between mock and shMRGPRX1 cells support a model where MRGPRX1 functions as a melanin synthesis suppressor. MRGPRX1 has emerged as a biologically significant pigmentation modulator by negatively regulating key melanogenic pathways, providing insights into research and clinical strategies in pigment biology. In this study, we examined the function of MRGPRX1, a G-protein coupled receptor family member, in epidermal melanogenesis and the underlying mechanisms in HEMs. In addition, we revealed the possibility that chloroquine acts as an agonist of MRGPRX1, an orphan receptor, and the mechanisms of chloroquine-induced hypopigmentation. These findings indicate that MRGPRX1 contributes to melanogenesis suppression, and antimelanogenesis is mediated by the MRGPRX1−TRPA1−CREB/p38 signaling pathway. We showed that chloroquine activates MRGPRX1 by acting as an agonist and then activates TRPA1−CREB/p38 signaling, leading to hypopigmentation. These results suggest that MRGPRX1 is a therapeutic target for treating pigmentary disorders.

MATERIALS AND METHODS

Cell culture

HEMs (C-102-5C, Gibco) were cultured in media 254 (M-254-500, Gibco) supplemented with 1% human melanocyte growth supplement (S-002-5, Gibco) and 1% streptomycin/penicillin (30-002-CI0, Corning) at 37 °C in a 5% carbon dioxide atmosphere with constant humidity, following previously described protocols (Yu et al, 2025).

In silico analysis

After verifying the isoform types using the UniProt Protein Database (https://www.uniprot.org), the structures of target proteins were retrieved from multiple sources. Structural information for human MC1R (UniProt identification: Q01726) and MRGPRX1 (UniProt identification: Q96LB2) was obtained from the Protein Data Bank (https://www.rcsb.org), SWISS-MODEL (https://swissmodel.expasy.org), and the AlphaFold Protein Structure Database (https://alphafold.ebi.ac.uk/). The chemical structures of FK (PubChem Compound Identification: 47936) and chloroquine (PubChem Compound Identification: 2719) were downloaded from the PubChem database (https://pubchem.ncbi.nlm.nih.gov/). Molecular docking simulations were conducted to estimate the binding affinity between the receptors and ligands, expressed as predicted free energy (kcal/mol). A semiflexible docking protocol was employed.

The predicted binding affinity is expressed in kcal/mol. Regarding software and program information for the in silico analysis, molecular docking was performed using a stochastic search algorithm (such as Lamarckian Genetic Algorithm) in AutoDock (version 4.2.6)

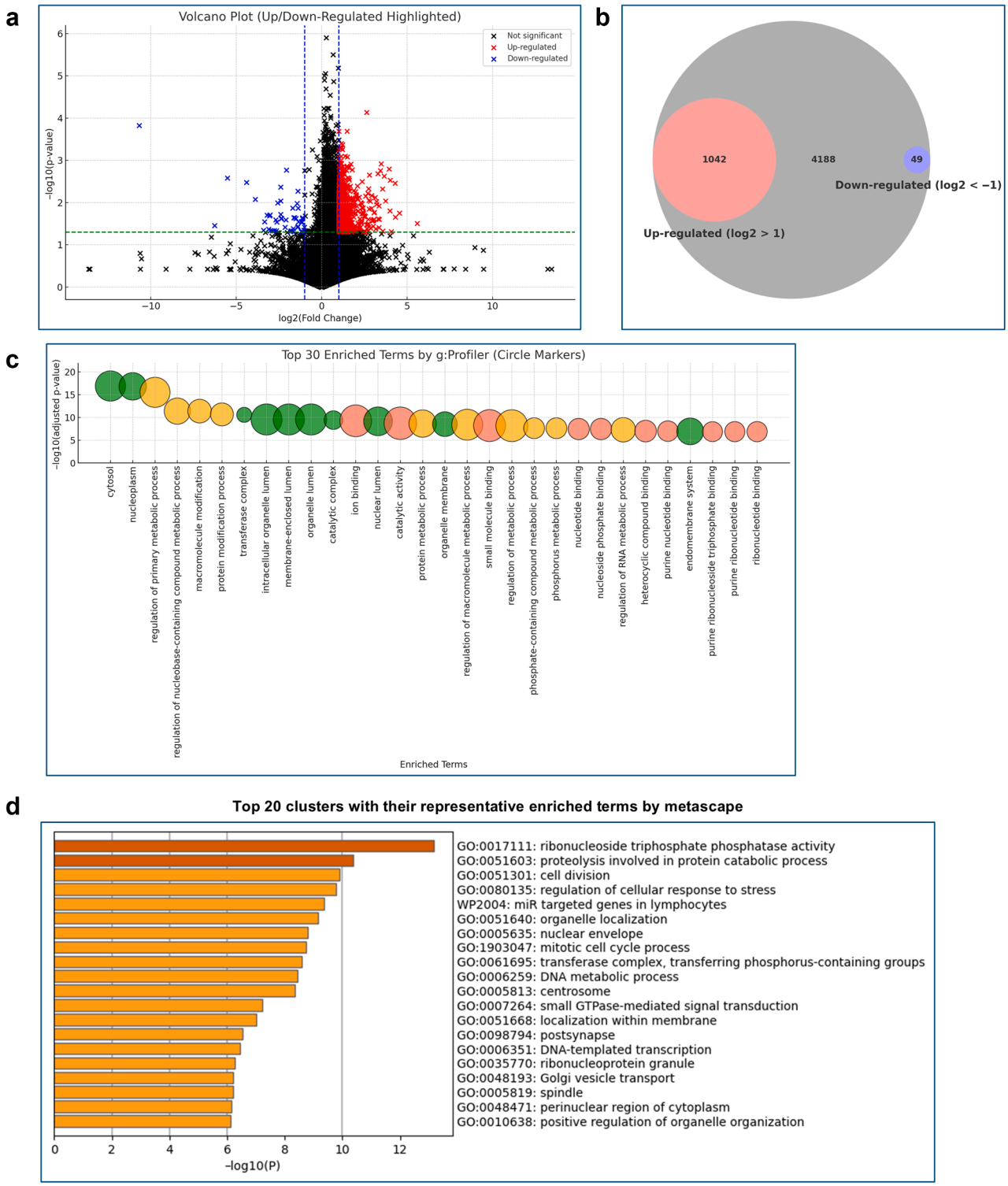

Figure 6. Transcriptome profiling and pathway analysis reveal potential involvement of MAPK and Wnt signaling in pigmentation-related gene regulation by MRGPRX1. **(a)** The volcano plot showing differentially expressed genes between mock- and shMRGPRX1-treated samples. Each point represents a single gene. The x-axis indicates the $\log_2$FC in expression between the 2 conditions, whereas the y-axis shows the statistical significance as $-\log_{10}$(*P*-value). Genes meeting the criteria of $\log_2$FC > 1 and $P < .05$ are classified as upregulated (red), whereas those with $\log_2$FC < -1 and $P < .05$ are classified as downregulated (blue). Genes with $-1 < \log_2$FC < 1 and $P < .05$ are considered not significantly changed in fold change (black). Dashed lines indicate the commonly used cutoffs of $\log_2$FC ± 1 (vertical) and $P = .05$ (horizontal). **(b)** Venn diagram illustrating gene groups from the volcano plot. The diagram shows the gene distribution on the basis of differential expression analysis. Blue represents downregulated genes, red indicates upregulated genes, and the black intersection includes genes with nonsignificant fold changes ($-1 < \log_2$FC < 1) but $P < .05$. **(c)** Top 30 enriched terms identified by g:Profiler, visualized as a bubble plot, where the x-axis represents enriched terms, the y-axis represents statistical significance ($-\log_{10}$ adjusted *P*-value), and bubble size reflects term size (number of associated genes). **(d)** Top 20 enriched terms from Metascape analysis, ranked by significance ($-\log_{10}$ *P*-value). Functional categories include GO biological processes, molecular

(Goodsell et al, 1996; Morris et al, 2009). The protein and chemical structures were docked using AutoDock Vina (version 1.2.3) (Trott and Olson, 2010) and AutoDockTools (Huey et al, 2012). Molecular docking enables modeling of protein−ligand interactions at the atomic level, allowing for prediction of the binding conformation and orientation of small molecules within the active site of target proteins.

Presto-TANGO luciferase reporter assay

HEK293T cells were transfected with 0.5 μg of each DNA type using polyethyleneimine solution. pCDNA3.1(+)-CMV-bArrestin2-TEV was gifted by Bryan Roth (Addgene, plasmid number 107245; http://n2t.net/addgene:107245; RRID:Addgene_107245) (Kroeze et al, 2015). MRGPRX1-Tango was also gifted from Bryan Roth (Addgene, plasmid number 66439; http://n2t.net/addgene:66439; RRID:Addgene_66439) (Kroeze et al, 2015). The Tet-inducible luciferase reporter was a gift from Moritoshi Sato (Addgene, plasmid number 64127; http://n2t.net/addgene:64127; RRID:Addgene_64127) (Nihongaki et al, 2015). β-Galactosidase plasmid DNA pSV-β-Galactosidase control vector (E108A, Promega) transfection was performed to confirm FLAG expression, and pSV-β-Galactosidase control vector was used as an internal control through the β-Galactosidase Enzyme Assay System.

ETHICS STATEMENT

Ethics approval was not applicable. No human or animal studies were conducted.

DATA AVAILABILITY STATEMENT

Data used to support the findings of this study are available from the corresponding author upon request. For data inquiries, the corresponding author (bioneer@skku.edu) should be contacted.

ORCIDs

Sae Woong Oh: http://orcid.org/0009-0008-3550-7027
Eunbi Yu: http://orcid.org/0009-0008-2939-7167
Kitae Kwon: http://orcid.org/0009-0004-8094-3531
Gyeonghyeon Kim: http://orcid.org/0009-0001-4322-8932
Hee Seon Shin: http://orcid.org/0009-0003-0873-5052
Seokhyeon Min: http://orcid.org/0009-0007-9683-8869
Yeonsoo Kim: http://orcid.org/0009-0004-0616-8071
Ki Wook Lee: http://orcid.org/0009-0005-7507-9811
Minkyung Song: http://orcid.org/0000-0003-2668-7528
Jae Youl Cho: http://orcid.org/0000-0001-8141-9927
Jongsung Lee: http://orcid.org/0000-0002-5073-2619

CONFLICT OF INTEREST

The authors state no conflict of interest.

ACKNOWLEDGMENTS

This study was supported by the Postdoctoral Research Program of Sungkyunkwan University (2023) and a grant from the Basic Science Research Program through the National Research Foundation of Korea funded by the Ministry of Science and Technology Information and Communication (grant number RS-2023-00246887) and a grant from the BK21 FOUR Project through the National Research Foundation of Korea. JL is the guarantor of this work.

AUTHOR CONTRIBUTIONS

Conceptualization: SWO, EY, MS, JYC, JL; Data Curation: SWO, EY, KK, GK, HSS, SM, KWL, YK; Formal Analysis: SWO, EY, KK, GK, HSS, SM, KWL, YK; Funding Acquisition: MS, JYC, JL; Methodology: KK, GK, HSS, SM, YK; Project Administration: JYC, JL; Resources: MS; Supervision: MS, JYC, JL; Validation: SWO, EY, MS; Writing − Original Draft Preparation: OSW, EY; Writing − Review and Editing: MS, JYC, JL

SUPPLEMENTARY MATERIAL

Supplementary material is linked to the online version of the paper at www.jidonline.org, and at https://doi.org/10.1016/j.jid.2025.09.016.

REFERENCES

Al Hamwi G, Riedel YK, Clemens S, Namasivayam V, Thimm DT, Müller CE. Mas-related G protein-coupled receptors X (MRGPRX): orphan GPCRs with potential as targets for future drugs. Pharmacol Ther 2022;238:108259.

Bader M, Alenina N, Andrade-Navarro MA, Santos RA. Mas and its related G protein−coupled receptors. Mrgprs. Pharmacol Rev 2014;66:1080−105.

Bowness JM, Morton RA. The association of zinc and other metals with melanin and a melanin-protein complex. Biochem J 1953;53:620−6.

D'Orazio JA, Nobuhisa T, Cui R, Arya M, Spry M, Wakamatsu K, et al. Topical drug rescue strategy and skin protection based on the role of Mc1r in UV-induced tanning. Nature 2006;443:340−4.

Dupré A, Ortonne JP, Viraben R, Arfeux F. Chloroquine-induced hypopigmentation of hair and freckles. Association with congenital renal failure. Arch Dermatol 1985;121:1164−6.

Goodsell DS, Morris GM, Olson AJ. Automated docking of flexible ligands: applications of AutoDock. J Mol Recognit 1996;9:1−5.

Huey R, Morris GM, Forli S. Using AutoDock 4 and AutoDock vina with AutoDockTools: a tutorial. The Scripps Research Institute Molecular Graphics Laboratory 2012;10550(92037):1000. URL: https://www.bch.cuhk.edu.hk/croucher11/tutorials/day1_autodock_tutorial.pdf. Accessed on: October, 2025.

Hwang YS, Oh SW, Park SH, Lee J, Yoo JA, Kwon K, et al. Melanogenic effects of maclurin are mediated through the activation of cAMP/PKA/CREB and p38 MAPK/CREB signaling pathways. Oxid Med Cell Longev 2019;2019:9827519.

Imamachi N, Park GH, Lee H, Anderson DJ, Simon MI, Basbaum AI, et al. TRPV1-expressing primary afferents generate behavioral responses to pruritogens via multiple mechanisms. Proc Natl Acad Sci USA 2009;106:11330−5.

Kiatsurayanon C, Niyonsaba F, Chieosilapatham P, Okumura K, Ikeda S, Ogawa H. Angiogenic peptide (AG)-30/5C activates human keratinocytes to produce cytokines/chemokines and to migrate and proliferate via MrgX receptors. J Dermatol Sci 2016;83:190−9.

Kroeze WK, Sassano MF, Huang X-P, Lansu K, McCorvy JD, Giguère PM, et al. Presto-Tango as an open-source resource for interrogation of the druggable human GPCRome. Nat Struct Mol Biol 2015;22:362−9.

Li Z, Tseng PY, Tiwari V, Xu Q, He SQ, Wang Y, et al. Targeting human Mas-related G protein-coupled receptor X1 to inhibit persistent pain. Proc Natl Acad Sci USA 2017;114:E1996−2005.

Martín-García RF, del R, Camacho NdR, Sánchez JL. Chloroquine-induced, vitiligo-like depigmentation. J Am Acad Dermatol 2003;48:981−3.

Meixiong J, Dong X. Mas-related G protein−coupled receptors and the biology of itch sensation. Annu Rev Genet 2017;51:103−21.

Morris GM, Huey R, Lindstrom W, Sanner MF, Belew RK, Goodsell DS, et al. AutoDock4 and AutoDockTools4: automated docking with selective receptor flexibility. J Comput Chem 2009;30:2785−91.

Nihongaki Y, Yamamoto S, Kawano F, Suzuki H, Sato M. CRISPR-Cas9-based photoactivatable transcription system. Chem Biol 2015;22:169−74.

Poyner DR, Hawkins PT, Benton HP, Hanley MR. Changes in inositol lipids and phosphates after stimulation of the MAS-transfected NG115-401L-C3 cell line by mitogenic and non-mitogenic stimuli. Biochem J 1990;271:605−11.

Saunders TS, Fitzpatrick TB, Seiji M, Brunet P, Rosenbaum EE. Decrease in human hair color and feather pigment of fowl following chloroquine diphosphate. J Invest Dermatol 1959;33:87−90.

Selvaag E. Chloroquine-induced vitiligo-like depigmentation. Ann Trop Paediatr 1997;17:45−8.

Solinski HJ, Petermann F, Rothe K, Boekhoff I, Gudermann T, Breit A. Human Mas-related G protein-coupled receptors-X1 induce chemokine receptor 2 expression in rat dorsal root ganglia neurons and release of chemokine ligand 2 from the human LAD-2 mast cell line. PLOS One 2013;8:e58756.

functions, cellular components, and pathway annotations (eg, WP, KEGG). GO, Gene Ontology; KEGG, Kyoto Encyclopedia of Genes and Genomes; log_2FC, log_2 fold change; shMRGPRX1, MRGPRX1-targeted short hairpin RNA; WP, WikiPathways.

Srivastav S, van der Graaf K, Jonnalagadda PC, Thawani M, McNew JA, Stern M. Motor neuron activity enhances the proteomic stress caused by autophagy defects in the target muscle. PLOS One 2024;19:e0291477.

Tatemoto K, Nozaki Y, Tsuda R, Konno S, Tomura K, Furuno M, et al. Immunoglobulin E-independent activation of mast cell is mediated by Mrg receptors. Biochem Biophys Res Commun 2006;349:1322–8.

Trott O, Olson AJ. AutoDock Vina: improving the speed and accuracy of docking with a new scoring function, efficient optimization, and multithreading. J Comput Chem 2010;31:455–61.

Yu E, Oh SW, Park S-H, Kwon K, Han SB, Kang SH, et al. The pigmentation of blue light is mediated by both melanogenesis activation and autophagy inhibition through OPN3–TRPV1. J Invest Dermatol 2025;145:908–18.e6.

SUPPLEMENTARY MATERIALS AND METHODS

Transfection (viral particle transduction)

Human embryonic kidney 293T cells were transfected with 6, 3, and 1.5 μg pLKO.1, psPAX2, and pMDG1, respectively, using polyethyleneimine solution. The psPAX2 plasmid was a gift from Didier Trono (Addgene, plasmid number 12260; http://n2t.net/addgene:12260; RRID: Addgene_12260). The pMD2.G plasmid was a gift from Didier Trono (Addgene, plasmid number 12259; http://n2t.net/addgene:12259; RRID: Addgene_12259). pLKO.1 puro was a gift from Bob Weinberg (Addgene, plasmid number 8453; http://n2t.net/addgene:8453; RRID:Addgene_8453) (Stewart et al, 2003). After 24 hours, the medium was replaced with a fresh medium; after another 24 hours, the supernatant was used for lentiviral particle concentration using a Lenti-X concentrator (631231, Takara). Lentiviral particles were transfected using 10 μg/ml polybrene (TR-1003-G, Sigma-Aldrich), and stably transfected cells were selected using puromycin (G264, Abcam).

Immunoblotting analysis

The cells were treated with chloroquine at the indicated concentrations. Protein samples were prepared using RIPA buffer (9806, Cell Signaling Technology). After washing with PBS, the cells were harvested in PBS by centrifuging at 15,000*g* and 4 °C for 3 minutes. The PBS was then removed, and the cells were incubated with RIPA buffer for 30 minutes on ice. The samples were then centrifuged at 15,000*g* and 4 °C for 15 minutes, and the supernatant was collected. Cell lysates were normalized using the Pierce bicinchoninic acid Protein Assay Kit (23225, Thermo Fisher Scientific). Then, 20 μg cell lysates were mixed with 4× sample buffer (161-0747, Bio-Rad Laboratories) and heated at 95 °C for 5 minutes. The samples were then separated using SDS-PAGE at 100 V for 1 hour. The proteins were then transferred onto polyvinylidene difluoride membranes (161-0177, Bio-Rad Laboratories) at 100 V for 60 minutes. The membranes were washed with Tris buffered saline with Tween buffer (200 mM Tris, 1500 mM sodium chloride, 0.01% Tween 20, pH 7.4), blocked with 2% BSA (A7906, Sigma-Aldrich) in Tris buffered saline with Tween buffer for 1 hour, and then incubated with specific antibodies on a shaking incubator at 4 °C for 16 hours. Protein bands were visualized using an enhanced chemiluminescence system (Amersham Biosciences) with horseradish peroxidase–conjugated antirabbit (A8919, Sigma-Aldrich) or antimouse (A0545, Sigma-Aldrich) secondary antibodies. After each antibody exposure, the membranes were washed with Tris buffered saline with Tween 4 times using an orbital shaker at 20 °C for 10 minutes. The results were confirmed in 3 independent experiments.

RNA extraction, DNA sample preparation, and RT-PCR analysis

Total RNA was isolated using the QIAzol lysis reagent (79306, Qiagen). The RNA was reverse transcribed using TOPscript RT DryMIX (RT200, Enzynomics) according to the manufacturer's instructions. The RT-PCR conditions were as follows: 3 minutes at 94 °C; 30 cycles of 15 seconds at 94 °C, 30 seconds at 60 °C, and 20 seconds at 72 °C; and a final step of 5 minutes at 75 °C. DNA samples were prepared using Taq polymerase PCR (P025A, Enzynomics). Each sample was mixed with 0.5 μl Taq polymerase, 2 μl 10× Taq buffer, 0.5 μl each of 100 μM forward and reverse primers, 1 μl cDNA, 4 μl dNTP, and 10.5 μl DEPC water. The Taq polymerase PCR conditions were 30 minutes at 50 °C; 40 cycles of 30 seconds at 95 °C, 30 seconds at 60 °C, and 30 seconds at 72 °C; and a final step of 5 minutes at 72 °C. DNA sample gel electrophoresis was performed on 1% agarose SYBR gel. The samples were mixed with 6× loading buffer and separated using agarose gel electrophoresis at 130 V for 20 minutes. The samples were visualized using an LED transilluminator (BK001, GeneDireX). The primers used were MRGPRX1 forward (CAC CAA TCA ACG GAA CTG AGG) and MRGPRX1 reverse (GAG GCT CAA GGT CTG CTT GTA).

RNA-sequencing library preparation, sequencing, and analysis

RNA sample preparation and RNA sequencing experiments with short hairpin RNA knockdown were prepared as described previously (Martin and Wang, 2011). Briefly, total RNA was isolated from normal human epidermal melanocytes transfected with either mock or MRGPRX1-targeted short hairpin RNA using standard protocols, followed by DNase treatment to remove genomic DNA. Polyadenylated RNA was enriched using the TruSeq Stranded mRNA Library Prep Kit (Illumina) and fragmented to an average size of 200–400 bp. First- and second-strand cDNA synthesis was performed, followed by adapter ligation and PCR amplification. Sequencing was performed on an Illumina platform with paired-end 101 bp reads. A total of 6 libraries ($n = 3$ per group) were generated and sequenced, yielding high-quality data (average Q30 > 97%). Adapter sequences and low-quality reads were removed using Trimmomatic (version 0.38), and read quality was confirmed using FastQC (version 0.11.7) (Bolger et al, 2014). Trimmed reads were aligned to the human reference genome (GRCh38) using HISAT2 (version 2.1.0), and transcript assembly was performed using StringTie (version 2.1.3b) (Kim et al, 2015; Pertea et al, 2016,2015). Gene expression levels were quantified as transcripts per kilobase million. Differentially expressed genes between mock- and MRGPRX1-targeted short hairpin RNA–treated cells were identified using DESeq2 with cutoffs of $|\log_2 \text{fold change}| \geq 1$ and $P < .05$.

Functional annotation

To investigate the biological relevance of differentially expressed genes, functional enrichment analysis was performed using the "Metascape" platform (Zhou et al, 2019). The analysis incorporated multiple ontology sources, including Gene Ontology, Kyoto Encyclopedia of Genes and Genomes, Reactome, and WikiPathways (Gene Ontology Consortium, 2004). Enriched Gene Ontology biological process terms were identified on the basis of cumulative hypergeometric distribution with a *P*-value threshold <.01. Terms were clustered using Kappa-statistical similarity scores, and representative terms from each cluster were selected. The resulting top 11 clusters highlighted key processes such as cell adhesion, immune signaling, and neurodevelopment. Enriched terms were visualized through heatmaps and

network plots, enabling the interpretation of functional relationships among differentially expressed genes. In parallel, STRING database (version 12.0) was used for functional enrichment analysis of differentially expressed genes (Szklarczyk et al, 2023). STRING enrichment included annotations from TISSUE-specific expression (on the basis of Human Protein Atlas data) and UniProt functional keywords.

Autophagic flux detection

Human embryonic kidney 293T cells were transfected with pMRX-IP-GFP-LC3-RFP-LC3ΔG, a gift from Noboru Mizushima (Addgene, plasmid number 84572; http://n2t.net/addgene:84572; RRID: Addgene_84572) using polyethyleneimine solution. Red and green fluorescence indicated internal control RFP-LC3ΔG and autophagic flux GFP-LC3, respectively.

Immunofluorescence analysis

Using the same laser power, the fluorescence intensities were measured. The results were determined using the ImageJ software (National Institutes of Health, version 1.50i) and ZEN 2012 Blue (Zeiss) under the same processing parameters.

Fluo-4 NW calcium assay

Cells were loaded with Fluo-4 NW dye solution prepared by adding 10 ml assay buffer and 100 μl probenecid stock solution (2.5 mM) to component A (Fluo-4 mix) of the Fluo-4 NW Calcium Assay Kit (Thermo Fisher Scientific). After removal of culture medium from 96-well plates, 100 μl dye solution was added to each well and incubated at 36 °C for 30 minutes followed by 30 minutes at room temperature. The dye solution was then replaced with assay buffer containing the indicated agonist or antagonist and prepared in advance, and cells were incubated for 10 minutes before measurement. Calcium fluorescence was recorded for 10∼20 minutes at minimal time intervals using 494/516 nm excitation/emission.

Determination of melanin content and cell viability assay

The melanin content of human epidermal melanocytes was measured as described by Huh et al (2010). Cells were cultured in 6-well plates until they reached 70−80% confluency, after which they were treated with chloroquine at the specified concentrations for 24 hours. After treatment, the cells were washed with PBS and incubated with 1 ml of 1 N sodium hydroxide for 16 hours at 20 °C. The resulting cell lysates were transferred to a microplate, and absorbance was measured at 405 nm using a Synergy STX microplate reader (BioTek). All measurements were conducted in triplicate and reported as means ± SD.

Cell viability was assessed using the Cell Counting Kit-8 (CK04, Dojindo). Cells at 70−80% confluency in 6-well plates were exposed to the indicated doses of chloroquine for 24 hours. The culture medium was then replaced with media 254 supplemented with 1% human melanocyte growth supplement (S-002-5, Gibco) and 1% streptomycin/penicillin (30-002-CI0, Corning). Subsequently, 5 μl of the Cell Counting Kit-8 reagent was added per well, and the cells were incubated for 2 hours at 37 °C in a 5% carbon dioxide humidified atmosphere. A 150 μl aliquot from each well was transferred to a microplate, and absorbance was measured at 450 nm using a BioTek microplate reader. All experiments were performed in triplicate and expressed as mean ± SD.

Tyrosinase activity

Cellular tyrosinase activity was determined as previously described by Huh et al (2010). Cells were seeded in 6-well plates and treated with chloroquine at the indicated concentrations for 24 hours. After treatment, cells were washed and collected by centrifugation at 15,000g for 5 minutes at 4 °C using 1.5 ml microcentrifuge tubes (MCT-175-C, Axygen). The resulting pellets were lysed by sonication for 30 seconds in tyrosinase lysis buffer (50 mM sodium phosphate buffer, pH 6.8, containing 1% Triton X-100 and 1 mM phenylmethanesulfonyl fluoride). After lysis, the cell extracts were centrifuged at 20,000*g* for 15 minutes at 4 °C, and the protein concentration in the supernatants was quantified using the Pierce bicinchoninic acid assay. A total of 100 μg of protein was incubated with 100 μl of dopachrome reaction buffer (50 mM sodium phosphate buffer, pH 6.8, and 2 mM L-DOPA, 333786, Sigma-Aldrich) at 37 °C for 15 minutes. The final reaction volume was adjusted to 300 μl using the lysis buffer. Tyrosinase activity in a cell-free system was assessed using the same protocol applied to untreated control cells. Dopachrome formation was quantified by measuring absorbance at 470 nm with a microplate reader (Synergy STX, BioTek). All assays were conducted in triplicate, and results are presented as mean ± SD.

Site-directed mutagenesis

Site-directed mutagenesis was performed using the Q5 Site-Directed Mutagenesis Kit (New England Biolabs) according to the manufacturer's instructions. Mutation-specific primers were designed using the NEBaseChanger tool by inputting the wild-type DNA sequence and defining the desired amino acid substitutions. PCR amplification was conducted with Q5 Hot Start DNA Polymerase, and the resulting products were subjected to a KLD (kinase−ligase−DpnI) treatment to phosphorylate the ends, ligate the DNA, and digest the parental template. The final product was transformed into chemically competent DH5alpha *E coli*. Mutagenesis strategies included alanine scanning to assess functional contribution of specific residues by eliminating side chain properties as well as charge-reversal and charge-neutralization mutations to investigate the role of electrostatic interactions in protein function.

Statistical analysis

All data are presented as mean ± SD. Statistical significance was determined using unpaired *t*-test or 1-way ANOVA compared with the control group in the Prism GraphPad software. $*P < .05$, $**P < .01$, and $***P < .001$.

SUPPLEMENTARY REFERENCES

Bolger AM, Lohse M, Usadel B. Trimmomatic: a flexible trimmer for Illumina sequence data. Bioinformatics 2014b;30:2114−20.

Huh S, Jung E, Lee J, Roh K, Kim JD, Lee J, et al. Mechanisms of melanogenesis inhibition by propafenone. Arch Dermatol Res 2010;302:561−5.

Gene Ontology Consortium. The Gene Ontology (GO) database and informatics resource. Nucleic Acids Res 2004;32(Suppl. 1):D258−61.

Kim D, Langmead B, Salzberg SL. HISAT: a fast spliced aligner with low memory requirements. Nat Methods 2015;12:357–60.

Martin JA, Wang Z. Next-generation transcriptome assembly. Nat Rev Genet 2011a;12:671–82.

Pertea M, Kim D, Pertea GM, Leek JT, Salzberg SL. Transcript-level expression analysis of RNA-seq experiments with HISAT, StringTie and Ballgown. Nat Protoc 2016;11:1650–67.

Pertea M, Pertea GM, Antonescu CM, Chang TC, Mendell JT, Salzberg SL. StringTie enables improved reconstruction of a transcriptome from RNA-seq reads. Nat Biotechnol 2015;33:290–5.

Stewart SA, Dykxhoorn DM, Palliser D, Mizuno H, Yu EY, An DS, et al. Lentivirus-delivered stable gene silencing by RNAi in primary cells. Rna 2003;9:493–501.

Szklarczyk D, Kirsch R, Koutrouli M, Nastou K, Mehryary F, Hachilif R, et al. The STRING database in 2023: protein–protein association networks and functional enrichment analyses for any sequenced genome of interest. Nucleic Acids Res 2023;51:D638–46.

Zhou Y, Zhou B, Pache L, Chang M, Khodabakhshi AH, Tanaseichuk O, et al. Metascape provides a biologist-oriented resource for the analysis of systems-level datasets. Nat Commun 2019;10:1523.

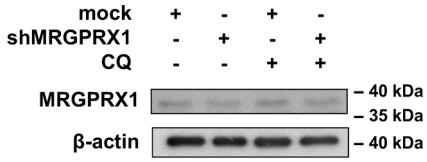

Supplementary Figure S1. MRGPRX1 immunoblotting results after shMRGPRX1 transduction. HEMs were transfected with shRNA and treated with 10 μM chloroquine for 48 h. HEM, human epidermal melanocyte; shMRGPRX1, MRGPRX1-targeted short hairpin RNA; shRNA, short hairpin RNA.

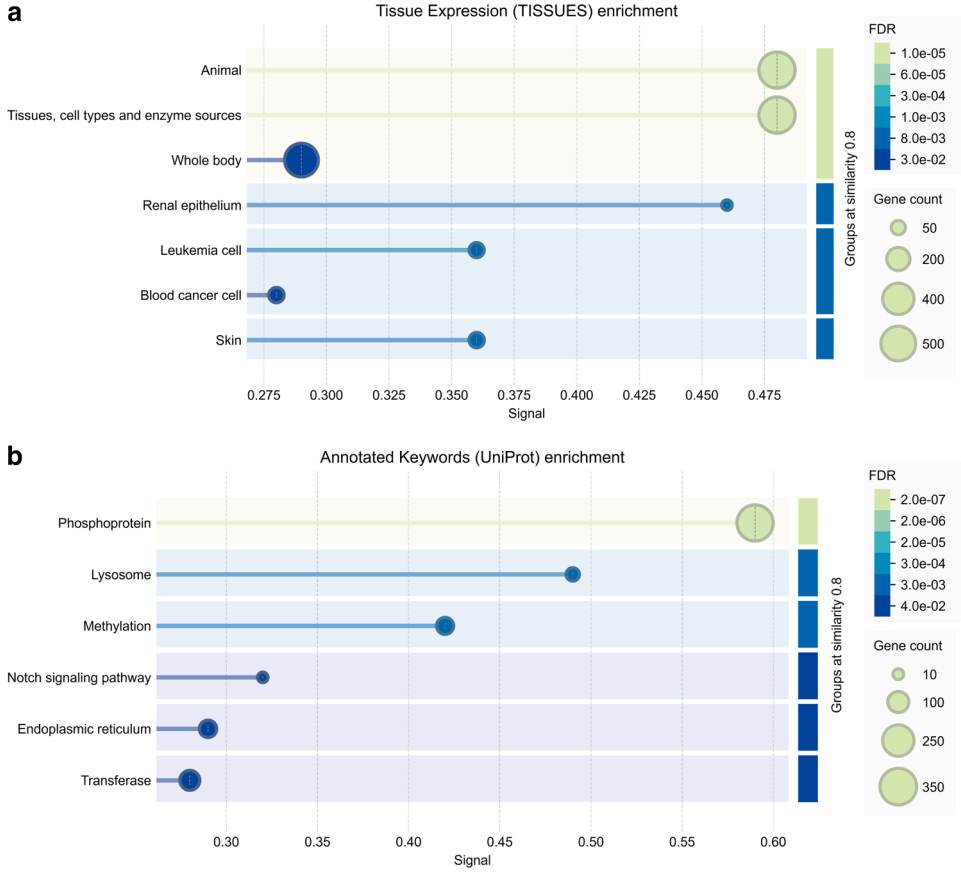

Supplementary Figure S2. STRING-based enrichment analysis of DEGs after MRGPRX1 knockdown. (**a**) Tissue-specific enrichment analysis based on expression profiles from the Human Protein Atlas. Genes differentially expressed between mock- and shMRGPRX1-transfected HEMn showed significant representation in tissue-specific gene sets, with the strong enrichment observed for skin-associated transcripts. The size of each circle indicates the number of genes associated with the given tissue, whereas color denotes the statistical significance of enrichment (FDR). The top terms were ranked on the basis of FDR, highlighting the relevance of tissue origin to the observed transcriptomic changes. (**b**) Functional category enrichment based on UniProt Keywords. DEGs were significantly enriched in functional classes such as "phosphoprotein" and "signal," suggesting active participation of signal transduction pathways and post-translational modifications in MRGPRX1-associated gene regulation. Circle size reflects the number of genes annotated with each keyword, and color scale indicates the adjusted *P*-value (FDR). These functional annotations support the hypothesis that MRGPRX1 knockdown affects extracellular signaling and intracellular phosphorylation cascades. DEG, differentially expressed gene; FDR, false discovery rate; HEMn, normal human epidermal melanocyte; shMRGPRX1, MRGPRX1-targeted short hairpin RNA.

Supplementary Table S1. Melanogenesis-Related Genes Ranked by Fold Change

Gene ID	Gene Symbol	Description	Gene Biotype	HGNC	MIM	*P*-Value	Fold Change	log2
4254	*KITLG*	KIT ligand	Protein coding	6343	184745	.14369	2.536709939	1.34295856
7474	*WNT5A*	Wnt family member 5A	Protein coding	12784	164975	.051603	2.257662353	1.17482974
4286	*MITF*	Melanocyte-inducing transcription factor	Protein coding	7105	156845	.011055	2.242852808	1.16533494
3815	*KIT*	KIT proto-oncogene, receptor tyrosine kinase	Protein coding	6342	164920	.008119	1.966312511	0.97549263
1499	*CTNNB1*	Catenin beta 1	Protein coding	2514	116806	.019087	1.830216746	0.87201451
283652	*SLC24A5*	Solute carrier family 24-member 5	Protein coding	20611	609802	.037013	1.765753299	0.82028379
1385	*CREB1*	cAMP responsive element binding protein 1	Protein coding	2345	123810	.060134	1.764651268	0.81938311
1638	*DCT*	Dopachrome tautomerase	Protein coding	2709	191275	.043478	1.758415004	0.8142756
7306	*TYRP1*	Tyrosinase related protein 1	Protein coding	12450	115501	.02902	1.739290881	0.79849923
2932	*GSK3B*	Glycogen synthase kinase 3 beta	Protein coding	4617	605004	.002787	1.665915809	0.73631549
2315	*MLANA*	Melan-A	Protein coding	7124	605513	.016453	1.505799607	0.59052979
5594	*MAPK1*	MAPK1	Protein coding	6871	176948	.012467	1.487121033	0.57252207
51176	*LEF1*	Lymphoid enhancer binding factor 1	Protein coding	6551	153245	.039771	1.480577426	0.56615994
1910	*EDNRB*	Endothelin receptor type B	Protein coding	3180	131244	.042297	1.379388127	0.46402845
7299	*TYR*	Tyrosinase	Protein coding	12442	606933	.017848	1.309601481	0.38912786
5077	*PAX3*	Paired box 3	Protein coding	8617	606597	.047899	1.279365672	0.35542868
4948	*OCA2*	OCA2 melanosomal transmembrane protein	Protein coding	8101	611409	.001272	1.231753303	0.30071334
5604	*MAP2K1*	MAPK1	Protein coding	6840	176872	.056881	1.209838089	0.27481399
652	*BMP4*	Bone morphogenetic protein 4	Protein coding	1071	112262	.021964	1.208024454	0.27264966
27022	*FOXD3*	Forkhead box D3	Protein coding	3804	611539	.217915	1.095722435	0.13188239

Abbreviations: CREB, CRE-binding protein; HGNC, HUGO Gene Nomenclature Committee; ID, identification; MIM, Mendelian Inheritance in Man.

Genes functionally associated with melanogenesis were manually selected on the basis of prior literature and pathway databases. The list includes genes involved in melanocyte differentiation, melanosome biogenesis, trafficking, and pigmentation. Genes were ranked in descending order of $\log_2$ fold change as observed in the transcriptomic dataset. Fold change and *P*-value correspond to differential expression between experimental and control groups.